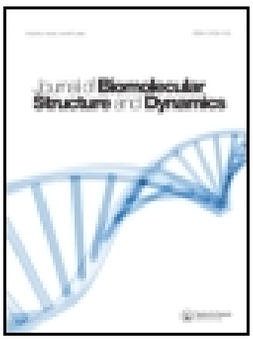

Taylor & Francis
Taylor & Francis Group

Journal of Biomolecular Structure and Dynamics

ISSN: (Print) (Online) Journal homepage: https://www.tandfonline.com/loi/tbsd20

N-{2-[(2-chlorothieno[3,2-d]pyrimidin-4-yl)amino]ethyl}-3-methoxybenzamide: design, synthesis, crystal structure, antiproliferative activity, DFT, Hirshfeld surface analysis and molecular docking study

Pei Huang , Juan Zhao , Yan-Hong Gao , Ling-Xia Jin , Qin Wang , Xiao-Hu Yu , Xiao-Hui Ji & Jiu-Fu Lu

To cite this article: Pei Huang , Juan Zhao , Yan-Hong Gao , Ling-Xia Jin , Qin Wang , Xiao-Hu Yu , Xiao-Hui Ji & Jiu-Fu Lu (2020): N-{2-[(2-chlorothieno[3,2-d]pyrimidin-4-yl)amino]ethyl}-3-methoxybenzamide: design, synthesis, crystal structure, antiproliferative activity, DFT, Hirshfeld surface analysis and molecular docking study, Journal of Biomolecular Structure and Dynamics, DOI: 10.1080/07391102.2020.1819424

To link to this article: https://doi.org/10.1080/07391102.2020.1819424

JOURNAL OF BIOMOLECULAR STRUCTURE AND DYNAMICS
https://doi.org/10.1080/07391102.2020.1819424

N-{2-[(2-chlorothieno[3,2-d]pyrimidin-4-yl)amino]ethyl}-3-methoxybenzamide: design, synthesis, crystal structure, antiproliferative activity, DFT, Hirshfeld surface analysis and molecular docking study

Pei Huang, Juan Zhao, Yan-Hong Gao, Ling-Xia Jin, Qin Wang, Xiao-Hu Yu, Xiao-Hui Ji and Jiu-Fu Lu

Shaanxi Key Laboratory of Catalysis, College of Chemical & Environment Science, Shaanxi University of Technology, Hanzhong, China

Communicated by Ramaswamy H. Sarma

ABSTRACT

The compound *N*-{2-[(2-chlorothieno[3,2-d]pyrimidin-4-yl)amino]ethyl}-3-methoxybenzamide (**8**) was synthesized by the condensation of 3-methoxybenzoic acid (**7**) with N^1-(2-chlorothieno[3,2-d]pyrimidin-4-yl)ethane-1,2-diamine (**6**). This intermediate was prepared from methyl 3-aminothiophene-2-carboxylate (**1**) by the condensation with urea, chlorination with phosphorus oxychloride and then condensation with ethane-1,2-diamine. The crystal structure of the title compound was determined and the crystal of the title compound belongs to the tetragonal system, space group *P4(3)* with $a = 9.4694(10)$ Å, $b = 9.4694(10)$ Å, $c = 18.886(3)$ Å, $\alpha = 90°$, $\beta = 90°$, $\gamma = 90°$. The optimized geometric bond lengths and bond angles obtained by using density functional theory (DFT) have been compared with X-ray diffraction values. The calculated HOMO and LUMO energies showed the character of the title compound. The molecular electrostatic potential (MEP) surface map of the related molecule was investigated with theoretical calculations at the B3LYP/6-311 + G(d,p) levels. A quantitative analysis of the intermolecular interactions in the crystal structures has been performed using Hirshfeld surface analysis. In addition, the title compound possesses marked inhibition against the proliferation of human colon cancer cell line HT-29 (IC_{50} = 1.76 μM), human lung adenocarcinoma cell line A549 (IC_{50} = 1.98 μM) and human gastric cancer cell line MKN45 (IC_{50} = 2.32 μM), displaying promising anticancer activitiy. The molecular docking studies revealed that the title compound may exhibit activity inhibiting PDB:3D15.

ARTICLE HISTORY
Received 30 July 2020
Accepted 29 August 2020

KEYWORDS
Thieno[3,2-d]pyrimidine; synthesis; X-ray diffraction; antiproliferative activity; Hirshfeld surface analysis

1. Introduction

Cancer has become one of the most life-threatening diseases to humans in the world for decades and has been the second most leading cause of disease-related deaths (Farce et al., 2004). Despite, enormous efforts to develop novel chemotherapeutic strategies to treat cancer, it still remains one of the major concerns worldwide. Most of the anticancer drugs currently in clinical use are limited in their therapeutic action due to their limited efficacy, non-specific toxicity, poor tolerance and the resistance demanding the necessity for the development of newer anticancer agents (Dörsam & Fahrer, 2016; Liu et al., 2019).

Thienopyrimidine derivatives are an important class of heterocyclic structures, and have received considerable attention in recent years due to their remarkable spectra of biological activities, such as antitumor (Heffron et al., 2010; Shi et al., 2019; Sutherlin et al., 2010), antioxidant (Kotaiah et al., 2012), anti-inflammatory (Rizk et al., 2012), antimicrobial (El-Sayed et al., 2012), antiviral properties (Bassetto et al., 2016). Among these active compounds, thieno[3,2-d]pyrimidine derivatives have been reported to show marked antitumor activities with different biotargets and mechanisms (Heffron et al., 2010; Sutherlin et al., 2010). For example, GDC-0941, which is a potent, selective, orally bioavailable inhibitor of PI3K, exerted antiprolifeative effects against an array of human tumor cell lines (Folkes et al., 2008). Further optimization of GDC-0941 led to several backup clinical candidates with similar structures, such as GNE-477 (Heffron et al., 2010), GNE-493 (Sutherlin et al., 2010), and GNE-490 (Sutherlin et al., 2010). In view of these observations of thieno[3,2-d]pyrimidine derivatives, and in continuation of our research program on the development of novel potent antitumor agents (Bravo-Altamirano et al., 2011; Ji et al., 2019; Lu, Jin, et al., 2017; Lu, Zhou, et al., 2017), a novel 4-thieno[3,2-d]pyrimidine derivative N-{2-[(2-chlorothieno [3,2-d]pyrimidin-4-yl)amino]ethyl}-3-methoxybenzamide (**8**) was designed and synthesized. The synthetic procedure for the title compound is shown in Scheme 1. To determinate the molecular structure and spatial absolute conformation, the single crystal was grown and tested by X-ray single-crystal diffraction. In addition, the biological tests suggested the compound displayed excellent antiproliferative activities on the proliferation of HT-29, A549 and MKN45 human cancer cell lines.

CONTACT Jiu-Fu Lu jiufulu@163.com Shaanxi Key Laboratory of Catalysis, College of Chemical & Environment Science, Shaanxi University of Technology, Hanzhong, 723001, China

Supplemental data for this article can be accessed online at https://doi.org/10.1080/07391102.2020.1819424.

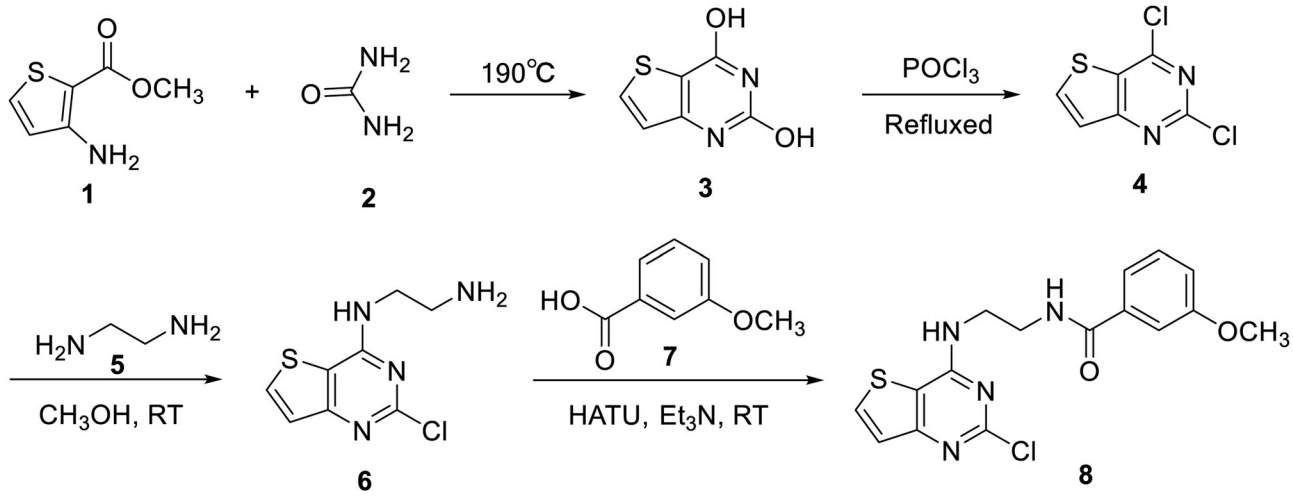

Scheme 1. Synthetic route of the title compound.

2. Experimental section

2.1. Physical measurements, chemicals, and reagents

Unless specified otherwise, all starting materials and reagents were obtained from commercial supplies without further purification. All melting points (°C) were taken on a Beijing Taike X-4 microscopy melting point apparatus and uncorrected. ^{1}H NMR spectra were recorded on a Bruker Biospin 600 MHz instrument using TMS as the internal standard. Mass spectra were recorded on a Waters Quattro micro API mass spectrometer (ESI, direct injection). All chemical shifts were reported in ppm. Elemental analysis of the synthesised compounds was carried out on a Carlo Erba 1108 analyser. Crystal data were obtained on a Bruker P4 X-diffractometer.

2.2. General procedure for synthesis of N-{2-[(2-chlorothieno[3,2-d]pyrimidin-4-yl)amino]ethyl}-3-methoxybenzamide (8)

2.2.1. Synthesis of thieno[3,2-d]pyrimidine-2,4-diol (3)

A mixture of methyl 3-amino-2-thiophenecarboxylate (50.5 g, 0.32 mol) and urea (96.5 g, 1.6 mol) was heated at 190 °C for 2.5 h. Upon cooling to about 120 °C, the reaction mixture was poured into sodium hydroxide (1000 mL, 1 N) solution and any insoluble material removed by filtration. The mixture was then acidified with 2 M HCl and a large amount of white solid was precipitated and filtered. The filter cake was dried to give 49.60 g of thieno[3,2-d]pyrimidine-2,4-diol (**3**) as a white solid. Yield: 91.8%. m.p. 102–104 °C (lit.[19] 102.9 °C). ESI-MS m/z: 167.1 $[M - H]^-$; ^{1}H NMR (300 MHz, DMSO-d_6) d: 6.93 (d, $J = 5.2$ Hz, 1H), 8.04 (d, $J = 5.2$ Hz, 1H), 11.19 (s, 1H), 11.61 (s, 1H).

2.2.2. Synthesis of 2,4-dichlorothieno[3,2-d]pyrimidine (4)

A mixture of thieno[3,2-d]pyrimidine-2,4-diol (22.2 g, 132.0 mmol), phosphorous oxychloride (150 mL) and catalytic amount DMF (0.5 mL) was heated at reflux for 12 h and the reaction was monitored by TLC. The reaction mixture was concentrated under reduced pressure and the residue was slowly added to ice/water with vigorous stirring. The mixture was then filtered to yield 18.9 g of 2,4-dichloro-thieno[3,2-d]pyrimidine (**4**) as a white solid. Yield: 69.8%. m.p. 139–141 °C (lit.[15] 138.8–139.3 °C); MS (ESI) m/z(%): 205.1 $[M + H]^+$.

2.2.3. Synthesis of N^1-(2-chlorothieno[3,2-d]pyrimidin-4-yl)ethane-1,2-diamine (6)

To the mixture of 2,4-dichloro-thieno[3,2-d]pyrimidine (8.0 g, 39.0 mmol) and MeOH (150 mL), ethane-1,2-diamine (11.7 g, 195.0 mmol) was added drop-wise at 0 °C. The reaction mixture then was stirred at room temperature for 7.5 h. After completion of reaction as indicated by TLC, the mixture was then filtered, washed with water and MeOH to yield 6.40 g of N^1-(2-chlorothieno[3,2-d]pyrimidin-4-yl)ethane-1,2-diamine (**6**) as a light yellow solid. Yield: 71.7%. m.p. >300 °C. MS (ESI) m/z(%): 229.1 $[M + H]^+$.

2.2.4. Synthesis of N-{2-[(2-chlorothieno[3,2-d]pyrimidin-4-yl)amino]ethyl}-3-methoxybenzamide (8)

Under N_2 atmosphere, a mixture of N^1-(2-chlorothieno[3,2-d]pyrimidin-4-yl)ethane-1,2-diamine (2.0 g, 8.75 mmol), 3-methoxybenzoic acid (1.46 g, 9.62 mmol), 1-[Bis(dimethylamino) methylene]-1*H*-1,2,3-triazolo[4,5-b] pyridinium 3-oxid hexafluorophosphate (HATU, 6.64 g, 17.49 mmol) and triethylamine (2.65 g, 26.24 mmol) in dried *N,N*-dimethylformamide (20 mL) was stirred at room temperature for 24 h. The reaction mixture was diluted with 10% Na_2CO_3 (100 mL), extracted by dichloromethane three times (80 mL × 3). The combined organic extracts was sequentially washed with 10% Na_2CO_3 (60 mL × 3) and brine (60 mL × 3) and dried over anhydrous Na_2SO_4. After evaporation of the organic solvent, the residue was recrystallized from ethyl acetate to afford 2.65 g of the title compound in 83.5% yields. mp 242 ~ 244 °C; ^{1}H NMR (600 MHz, DMSO-d_6) δ 8.61 (t, $J = 5.5$ Hz, 1H), 8.49 (t, $J = 5.5$ Hz, 1H), 8.17 (d, $J = 5.3$ Hz, 1H), 7.46–7.29 (m, 4H), 7.12–7.05 (m, 1H), 3.79 (s, 3H), 3.68–3.61 (m, 2H), 3.56–3.50 (m, 2H); MS (ESI) m/z(%): 363.1$[M + H]^+$, 385.1$[M + Na]^+$; Anal. calcd for $C_{16}H_{15}ClN_4O_2S$: C 52.97, H 4.17, N 15.44; found C 53.08, H 4.23, N 15.56.

Table 1. Hydrogen bond lengths (Å) and bond angles (°).

D–H···A	d(D–H)	d(H···A)	d(D···A)	∠DHA
N(4)-H(4)···O(1) #1	0.86	2.12	2.912(5)	152
N(3)-H(3)···N(1) #2	0.86	2.14	2.944(5)	156

Symmetry codes: (#1) y, -x + 2, -z + 1/4; (#2) -y + 2, x-1, z-1/4.

Table 2. Geometric parameters of the title compound.

Bond lengths	X-ray	Bond angles	X-ray
C(1)-C(2)	1.380(5)	C(2)-C(1)-C(4)	118.4(4)
C(1)-C(4)	1.415(5)	C(2)-C(1)-S(1)	111.8(3)
C(1)-S(1)	1.719(4)	C(4)-C(1)-S(1)	129.7(3)
C(2)-N(1)	1.367(5)	N(1)-C(3)-N(2)	131.3(4)
C(3)-N(1)	1.309(5)	N(1)-C(3)-Cl(1)	114.8(3)
C(3)-Cl(1)	1.751(4)	N(3)-C(4)-N(2)	118.5(4)
C(4)-N(3)	1.335(5)	O(1)-C(9)-C(10)	121.1(4)
C(4)-N(2)	1.346(5)	N(4)-C(9)-C(10)	117.9(3)
C(7)-N(3)	1.453(5)	C(11)-C(10)-C(15)	119.5(4)
C(8)-N(4)	1.452(4)	C(3)-N(1)-C(2)	112.8(4)
C(9)-O(1)	1.238(5)	C(3)-N(2)-C(4)	116.0(4)
C(9)-N(4)	1.336(5)	C(4)-N(3)-C(7)	123.6(3)
C(9)-C(10)	1.492(5)	C(12)-O(2)-C(16)	117.6(4)
C(10)-C(11)	1.380(6)	Torsion angles	
C(10)-C(15)	1.384(5)	N(3)-C(4)-N(2)-C(3)	178.8(4)
C(12)-O(2)	1.355(5)	N(4)-C(9)-C(10)-C(11)	10.4(6)
C(16)-O(2)	1.435(5)	C(7)-C(8)-N(4)-C(9)	−82.9(4)

2.3. Crystal data structure determination

The yellow powder of the title compound was dissolved in ethanol/ethyl acetate/tetrahydrofuran (1/1/1 by V/V/V). After slowly evaporating the solvents for several days, some single crystals suitable for X-ray analysis were obtained. A light yellow crystal ($C_{16}H_{15}ClN_4O_2S$) with dimensions of 0.20 mm × 0.18 mm × 0.15 mm was selected for data collection which was performed on a Bruker APEX-II CCD automatic diffractometer with a graphite-monochromatic Mo *Ka* radiation ($\lambda = 0.71073$ Å) by using the φ and ω-scan mode at 293 K. A total of 8693 reflections were collected in the range of $2.40 < \theta < 25.00°$ (index ranges: $-11 < h < 9$, $-11 < k < 11$, $-22 < l < 22$) and 2975 were independent ($R_{int} = 0.032$), of which 2429 observed reflections with $I > 2\sigma(I)$ were used in the structure determination and refinements. The structure was solved by direct methods with SHELXS-97 program (Sheldrick, 1997) and expanded by Fourier technique. The non-hydrogen atoms were refined anisotropically. The hydrogen atoms bound to carbon were determined with theoretical calculations and those attached to nitrogen and oxygen were determined with successive difference Fourier syntheses. The structure was refined by full-matrix Least-squares techniques on F^2 with SHELXL-97 (Sheldrick, 1997). The final refinement gave the final $R = 0.038$ and $wR = 0.066$ ($w = 1/[\sigma^2(F_o^2) + (0.010P)^2 + 0.5337P]$, where $P = (F_o^2 + 2F_c^2)/3$). $S = 1.08$, $(\Delta/\sigma)_{max} < 0.001$, $(\Delta\rho)_{max} = 0.22$ and $(\Delta\rho)_{min} = -0.17$ e/Å^{-3}. The hydrogen bond data and geometric parameters of title compound are listed in Table 1 and Table 2, respectively.

2.4. In vitro antiproliferative activity test of the title compound on HT-29, A549 and MKN45 cell lines

The named compound **8** was evaluated for its *in vitro* antiproliferative activity against three cancer cell lines (human colon cancer cell line HT-29, human lung adenocarcinoma cell line A549 and human gastric cancer cell line MKN45) by the MTT-based assay using sorafenib tosylate as a positive control. Cells were grown in 96-well culture plates. The tested compounds of various concentrations were added into the plates at 37 °C with 5% CO_2. After 72 h treatment, the medium was removed. Cells were treated with 20 μL fresh MTT solution for 3∼4 h at 37 °C. The medium was replaced by 150 μL dimethyl sulfoxide and the absorbance was measured on a microplate reader at 492 nm. The results were expressed as IC_{50} (inhibitory concentration 50%) and calculated by using the Bacus Laboratories Incorporated Slide Scanner (Bliss) software.

2.5. Dft calculations

Theoretical DFT analysis of **8** for its structure and reactivity was done by using Gaussian 09 program package at DFT/B3LYP/6-311 + G(d,p) method/basis set (Becke, 1993; Frisch et al., 2009; Lee et al., 1988). The geometry of **8** was optimized and quantum parameters were computed. Frontier molecular orbitals (FMO), molecular electrostatic potential (MEP) and band gap were also computed at B3LYP/6-311 + G(d,p) method/basis set of theory.

2.6. Hirshfeld surface calculations

Crystal Explorer program 17.5 was employed to carry out the Hirshfeld surface analysis. It showed that the possible molecular packing and hydrogen bond interactions in the structure (Turner et al., 2017). The structural input file was obtained in the CIF format. Hirshfeld surface distance from the nearest nucleus inside and outside the surface was measured and represented by d_i and d_e, respectively, while a normalized contact distance was represented as d_{norm}. White, red and blue colors have been selected for the visualization of d_{norm}.

2.7. Docking study

To understand the binding mode of the novel 4-thieno[3,2-d]pyrimidine derivative, docking analysis was performed by AutoDock 4.2.6 using the default docking parameters (Morris et al., 2009). The maps were generated by AutoGrid 4.2.6 with a spacing of 0.375 Å. Compound **8** was docked with protein of mouse Aurora A (Asn186->Gly, Lys240->Arg, Met302->Leu) in complex with 1-(3-chloro-phenyl)-3-{[2-(thieno[3,2-d]pyrimidin-4-ylamino)-ethyl]-thiazol-2-yl}-urea (PDB ID code: 3D15) at the active site of the public domain crystal structure for an analogue AK2. The results of docking was visualized with PyMOL 1.8.

3. Results and discussion

3.1. Description of the crystal structure of 8

The synthetic route of the title compound in four steps with good yield was depicted in Scheme 1. The ^{1}H NMR, MS, elemental analysis and X-ray diffraction data for the product

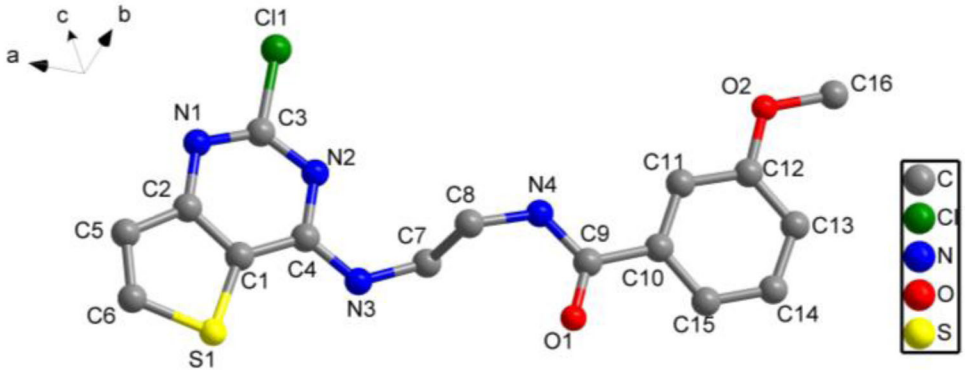

Figure 1. Structure of the title compound ($C_{16}H_{15}ClN_4O_2S$) with all non-H atom-labelling scheme and ellipsoids drawn at the 30% probability level.

Table 3. *In vitro* anticancer activity test[a] of the title compound on HT-29, A549 and MKN45 cell lines.

	IC_{50} IC_{50}/(μmol·L^{-1})		
Compound	HT-29	A549	MKN45
The title compound	1.76	1.98	2.32
Sorafenib Tosylate	3.81	2.62	3.58

[a]Test MTT colourimetric assay in HT-29, A549 and MKN45 human cancer cell lines. Each experiment was carried out in triplicate.

are in good agreement with the structure of the title compound. According to X-ray analysis, compound 6 crystallizes in tetragonal system, space group P4(3). As shown in Figure 1, the molecular structure of $C_{16}H_{15}ClN_4O_2S$, (**1**), consists of a central pyrimidine ring which is significantly puckered to assume a screw-boat conformation fused to a thiophene ring with imino group and chlorine bonded at the C3 and C4 positions, respectively, around this fused-ring thieno[3,2-d]pyrimidine moiety. The dihedral angle between the mean planes of the thieno[3,2-d]pyrimidine and benzene ring (C(10)∼C(15)) is 4.264°, which means the fused thieno[3,2-d]pyrimidine ring and benzene ring (C(10)∼C(15)) are nearly in the same plane. In the crystal, the average bond lengths and bond angles of benzene rings and thieno[3,2-d]pyrimidine are in normal ranges. The C(3)–N(1) (1.309(5) Å) and C(3)–N(2) (1.321(5) Å) bonds are significantly shorter than a normal single C–N bond (1.47 Å) and longer than a C = N bond (1.28 Å), indicating significant electron delocalization in the thieno[3,2-d]pyrimidine ring system. On the other hand, a mass of Intermolecular hydrogen bonds typed N–H···O and N–H···N are found in the crystal structure of the title compound (See Table 3), which play a major role in stabilizing the molecule. Atoms O(1)#1 and N(1)#2 act as hydrogen-bond donors, via H(4)–N(4) and H(3)–N(3), to generate the supramolecular structure (Figure 2).

3.2. Anticancer activity evaluation

In addition, the bioassay results showed the title compound **8** showed remarkable antiproliferative activity against HT-29, A549 and MKN45 cell lines with IC_{50} values of 1.76 μM, 1.98 μM and 2.32 μM, respectively, and thus it was slightly more potent than sorafenib tosylate (Table 3). Further structure optimization may result in more active anticancer compounds. Further studies on structural optimization and biological activities about these derivatives are still underway in our laboratory and will be reported in the future.

3.3. Computational DFT studies

The optimized geometry and electronic parameters (bond lengths, bond angles, E_{HOMO}, E_{LUMO}) of compound **8** were done using B3LYP/6-311 + G(d,p) level of theory. The optimized geometry and HOMO-LUMO orbitals of compound **8** are given in Figure 3. Obviously, the optimized structure results are consistent with X-ray diffraction data. The global energy minimum obtained by DFT of the structure optimization is −1846.917254 Hartree (-4.849×10^6 kcal·mol^{-1}). And the geometrical parameters such as bond length and bond angles related to studied compound are presented in detail, which are well replicated with the experimental data according to X-ray single-crystal diffraction. It can be seen from the results provided in Table 4. The minor deviations between theoretical and experimental results are due to differences in the molecular environment. It should be noted that XRD results were obtained in the crystalline phase. On the other hand, theoretical calculations were made in the gas phase using Gaussian Program. Significantly, experimental and theoretically obtained geometric parameter values are very close to each other (for example C3-N1 bond length values are 1.309 (5) and 1.309, respectively).

To predict the molecular transitions, the frontier molecular orbital (FMO) analysis was carried out by using the quantum mechanical approach reported (Barakat et al., 2015; Sıdır et al., 2010). E_{HOMO} and E_{LUMO} values give an estimate of the inevitable charge exchange collaboration inside the studied material. Dipole moment (μ), electronegativity (χ), hardness (η), electrophilicity (ω) and softness (σ) are recorded in Table 5. The highest occupied molecular orbital energy determines the electron-donating ability. However, the lowest unoccupied molecular orbital energy provides the ability of a molecule to accept an electron (Sakthivel et al., 2018). The corresponding E_{HOMO} and E_{LUMO} values were found to be −6.513 eV and −1.722 eV, respectively. The significances of η and σ are evaluated both the reactivity and stability.

The molecular electrostatic potential (MEP) was defined in terms of total charge distribution of a molecule. The optimized geometry at the B3LYP/6-311 + G(d,p) level of theory was used to map the molecular electrostatic potential

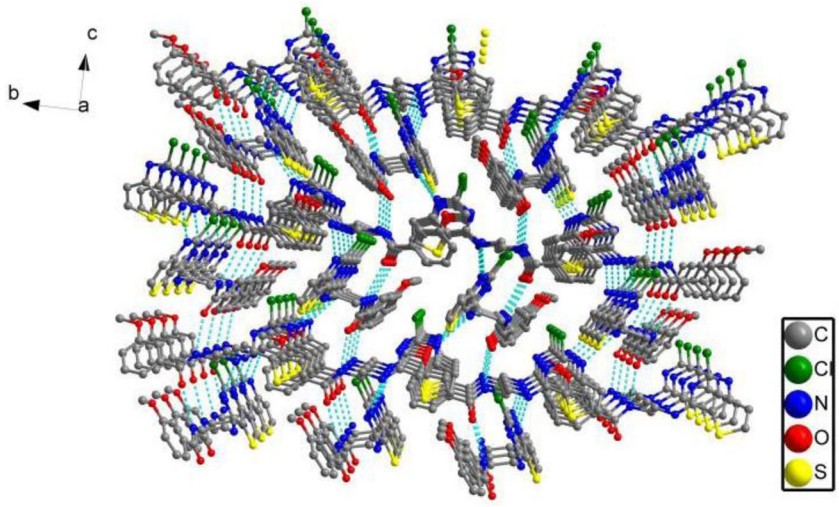

Figure 2. A packing diagram of the title compound ($C_{16}H_{15}ClN_4O_2S$).

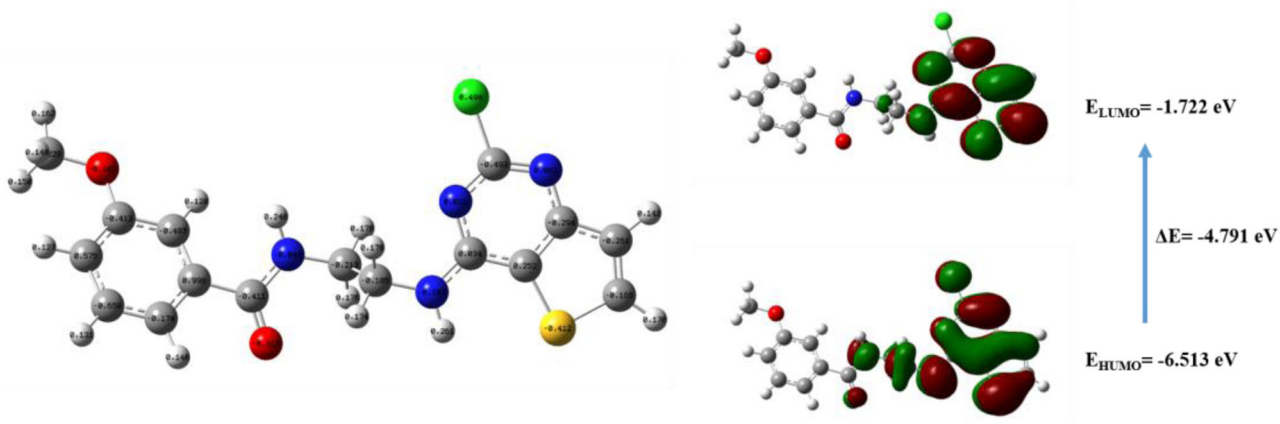

Figure 3. Left: the optimized geometry of **8** at the B3LYP/6-311 + G(d,p) level of theory, Right: HOMO, LUMO, E_{HOMO}, E_{LUMO} and bandgap (ΔE).

surface (MEPS) of the compound **8** by Multiwfn (Lu & Chen, 2012) and VMD (Humphrey et al., 1996), as shown in Figure 4. It helps to investigate the interaction between molecules, predict reaction sites and predict molecular property. The electron density is essential for understanding the electrophilic or nucleophilic reactivity as well as non-bonding interactions (Hartwar et al., 2015) At the MEP surface, different colours represent the different electrostatic potential values. Red and blue indicate electron-rich and electron-poor regions, and white indicates zero electrostatic potential.

3.4. Hirshfeld surface analysis

The Hirshfeld surface (HS) analysis of compound **8** was carried out by using Crystal Explorer 17.5 to investigate the weak intermolecular interactions. Figure 5a presents 3D Hirshfeld surface and electrostatic potentials surface maps generated for compound **8**. The white colour indicates medium proximity of out side atoms, and the red and blue colours indicate close or little proximity. Red spots on Hirshfeld surface are related to the hydrogen bonding interactions. As shown in Figure 5(a), the red region on Hirshfeld surface which is prominent above the oxygen atom (O1) in the N—H···O contacts and the nitrogen atoms (N1, N3, N4) in the N—H···N, N—H···N and N—H···O contacts, respectively.

The shape-index of the HS can visualize weak π···π stacking interactions by the presence of adjacent red and blue triangles. If there are no adjacent red and/or blue triangles, then there are no π···π interactions. Figure 5(b) clearly suggests that there are π···π interactions in the titled compound. The intermolecular interactions appear as distinct spikes in the 2 D fingerprint plots are illustrated in Figure 6(a–i), which are generated correspond to the H···H, H···C/C···H, H···N/N···H, H···O/O···H, H···S/S···H, H···Cl/Cl···H, C···N/N···C and C···O/O···C mutual effects (Mckinnon et al., 2004). To provide context, the complete fingerprint contour is displayed in gray and blue areas showing separate contacts. According to the fingerprint plots, the most important interaction is H···H interactions accounting for 32.9% of the total area of the Hirshfeld surfaces. In the presence of a weak C—H···π interaction in the crystal, a pair of characteristic wings appear in the fingerprint plot delineated into H···C/C···H contacts with a 13.2%. In addition, the proportions of H···N/N···H, H···O/O···H, H···S/S···H, H···Cl/Cl···H, C···N/N···C and C···O/O···C interactions comprised 9.6%, 8.7%, 6.5%,

14.8%, 1.5% and 1.7% of the HS surface, respectively. The results showed that van der Waals interactions, weak intermolecular interactions and hydrogen bonding make the structure more stable (Zhou et al., 2019).

Table 4. Some selected experimental and theoretical geometric parameters for Compound **8**.

Geometric parameters	Experimental [X-ray diffraction]	Theoretical [DFT/B3LYB]
C(1)-C(2)	1.380(5)	1.401
C(1)-C(4)	1.415(5)	1.415
C(1)-S(1)	1.719(4)	1.747
C(2)-N(1)	1.367(5)	1.356
C(3)-N(1)	1.309(5)	1.309
C(3)-Cl(1)	1.751(4)	1.763
C(4)-N(3)	1.335(5)	1.356
C(4)-N(2)	1.346(5)	1.34
C(7)-N(3)	1.453(5)	1.459
C(8)-N(4)	1.452(4)	1.455
C(9)-O(1)	1.238(5)	1.255
C(9)-N(4)	1.336(5)	1.367
C(9)-C(10)	1.492(5)	1.504
C(10)-C(11)	1.380(6)	1.393
C(10)-C(15)	1.384(5)	1.401
C(12)-O(2)	1.355(5)	1.364
C(16)-O(2)	1.435(5)	1.422
Bond angles		
C(2)-C(1)-C(4)	118.4(4)	117.847
C(2)-C(1)-S(1)	111.8(3)	111.703
C(4)-C(1)-S(1)	129.7(3)	130.45
N(1)-C(3)-N(2)	131.3(4)	129.732
N(1)-C(3)-Cl(1)	114.8(3)	115.88
N(3)-C(4)-N(2)	118.5(4)	118.254
O(1)-C(9)-C(10)	121.1(4)	121.741
N(4)-C(9)-C(10)	117.9(3)	116.539
C(11)-C(10)-C(15)	119.5(4)	119.754
C(3)-N(1)-C(2)	112.8(4)	113.795
C(3)-N(2)-C(4)	116.0(4)	117.41
C(4)-N(3)-C(7)	123.6(3)	123.788
C(12)-O(2)-C(16)	117.6(4)	118.63
Torsion angles		
N(3)-C(4)-N(2)-C(3)	178.8(4)	179.346
N(4)-C(9)-C(10)-C(11)	10.4(6)	24.807
C(7)-C(8)-N(4)-C(9)	−82.9(4)	−79.052

Table 5. Quantum chemical parameters of the investigated molecule using DFT method.

	μ (Debye)	IP (eV)	EA (eV)	χ (eV)	η (eV)	ω (eV)	σ (eV)
DFT	2.7878	6.513	1.722	4.118	2.396	3.539	0.283

The individual intermolecular interactions described above can also be visualized by the different Hirshfeld surface representations with the function d_{norm} plotted onto the surface. As shown in Figure 7(a–f), H···H, H···C/C···H, H···N/N···H, H···O/O···H, H···S/S···H and H···Cl/Cl···H interactions were revealed. The Hirshfeld surface analysis provides a full understanding of the intermolecular interactions in a facile and immediate way.

3.5. Docking study

Docking study is a very important technique in structure-based drug design. The method can estimate the conformation pattern of binding within the target protein (Anderson, 2003; Gilbert, 2004). Docking was performed by AutoDock 4.2.6 using the default docking parameters. Firstly, compound **8** having medical and pharmacological importance was optimized with B3LYP/6-311 + G(d,p) method/basis set and recorded as Protein Data Bank (PDB) format. In second step, compound **8** was docked with protein of mouse Aurora A (Asn186->Gly, Lys240->Arg, Met302->Leu) in complex with 1-(3-chloro-phenyl)-3-{[2-(thieno[3,2-d]pyrimidin-4-ylamino)-ethyl]-thiazol-2-yl}-urea (PDB ID code: 3D15) at the active site of the public domain crystal structure for an analogue AK2 (Dabrowska & Brylinski, 2006; Dilly & Liegeois, 2016; Duan et al., 2003; Kang et al., 2016). The active sites of protein PDB:3D15 were determined as HIS-214, PHE-213, TYR-212, GLY-211, GLN-140, ILE-222, TRP-141, ARG-139, TYR-210 and PHE-146 active residues. The spacing of grid boxes is 0.375 Å. The obtained docking result for compound **8**-PDB:3D15 was given in Figure 8. The binding was determined with −5.78 kcal/mol energy (ΔG) and three active hydrogen bonding. The inhibition constants for compound **8** and PDB:3D15 interactions (Ki) was calculated as 57.96 μM. As shown in Figure 8, the O1, H14, H15 atom in compound 8 docked well with the protein residues TRP-141, ARG-139 and TYR-210 via H-bond, respectively.

4. Conclusion

A novel 4-thieno[3,2-d]pyrimidine derivative, named *N*-{2-[(2-chlorothieno [3,2-d]pyrimidin-4-yl)amino]ethyl}-3-methoxy-benzamide has been synthesized and its structure was

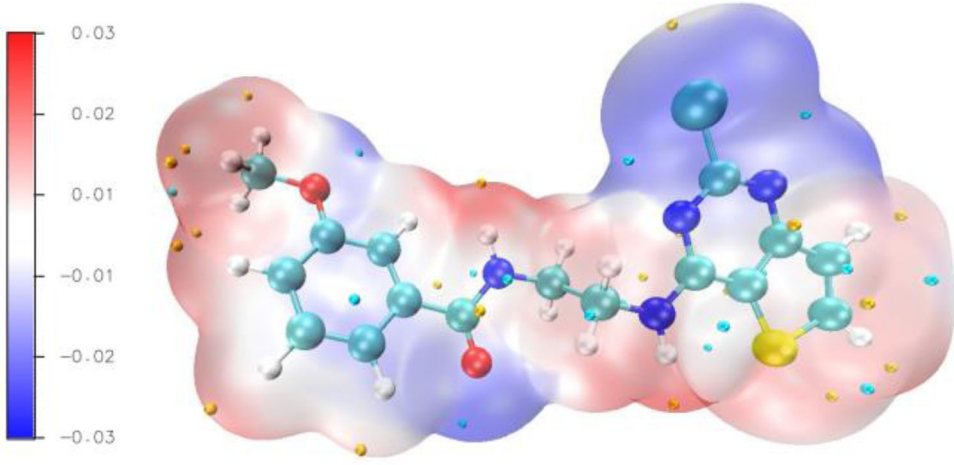

Figure 4. Molecular electrostatic potential surfaces (MESP, a.u.) of compound **8**.

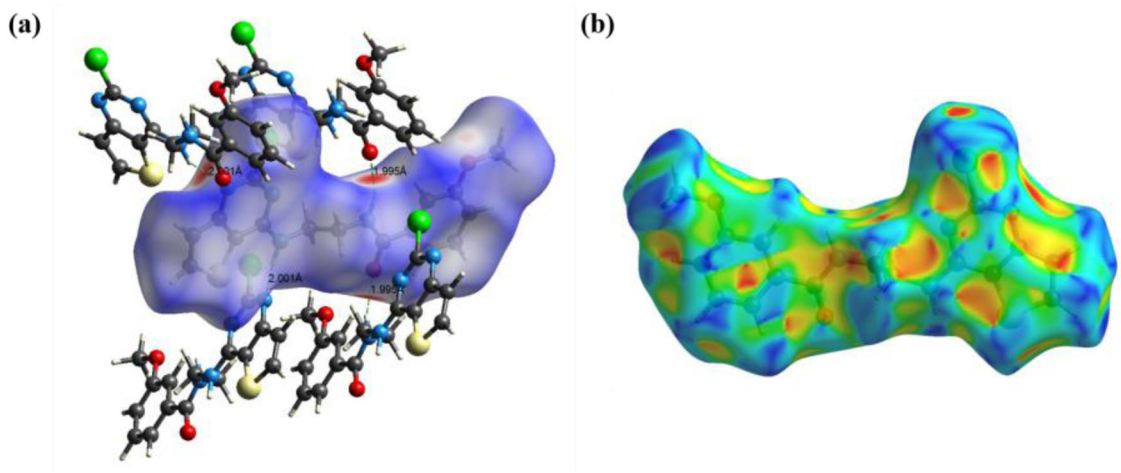

Figure 5. (a) View of the three-dimensional Hirshfeld surface of compound **8** plotted over d_{norm} in the range -0.4862 to 1.3170 a.u.; (b) Hirshfeld surface of compound **8** plotted over shape-index.

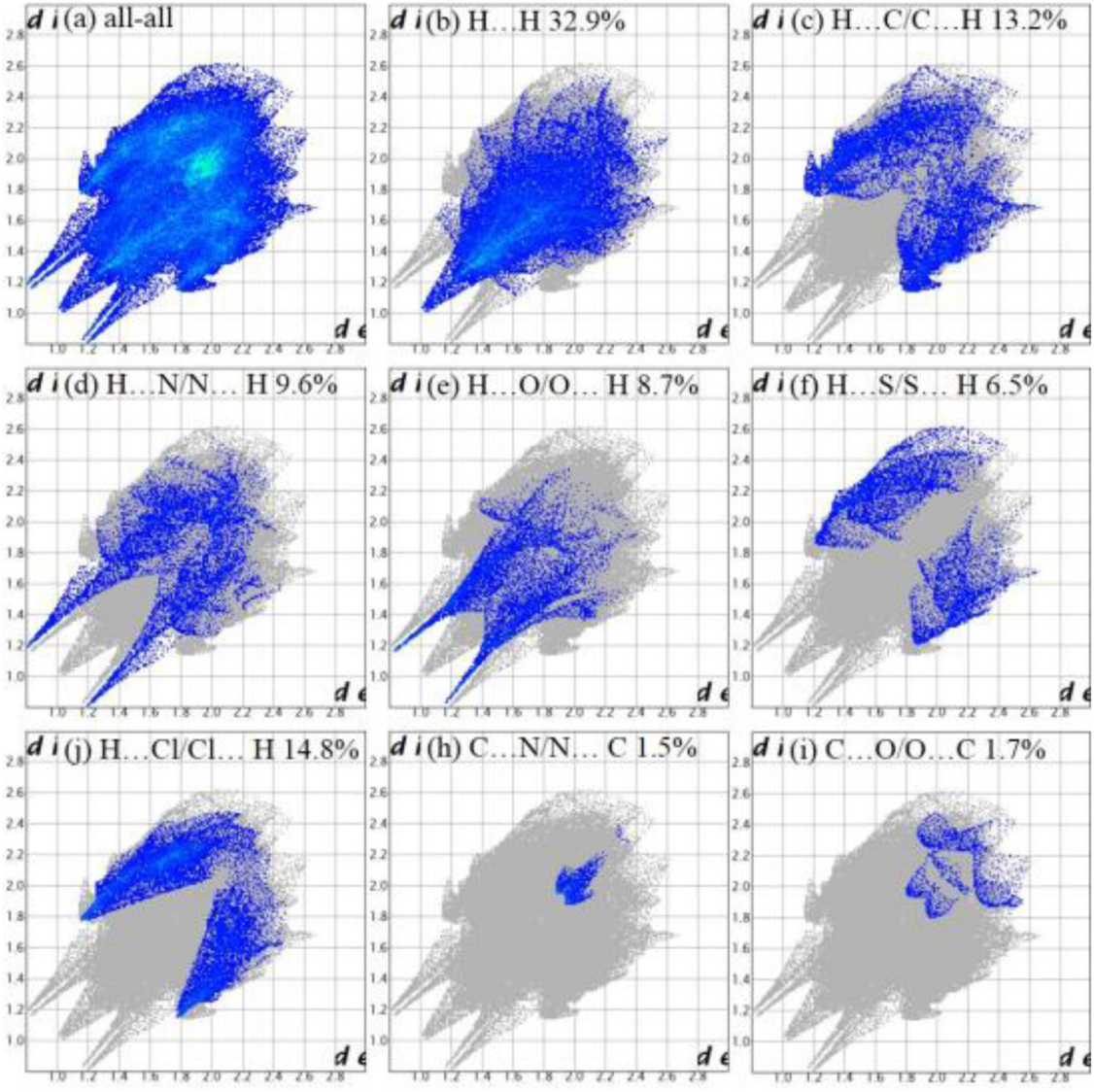

Figure 6. The full two-dimensional fingerprint plots for compound **8**, showing (a) all interactions, and delineated into, (b) H···H, (c) H···C/C···H (d) H···N/N···H, (e) H···O/O···H, (f) H···S/S···H, (g) H···Cl/Cl···H, (h) C···N/N···C, (i) C···O/O···C. The d_i and d_e values are the closest internal and external distances (in Å) from given points on the Hirshfeld surface contacts.

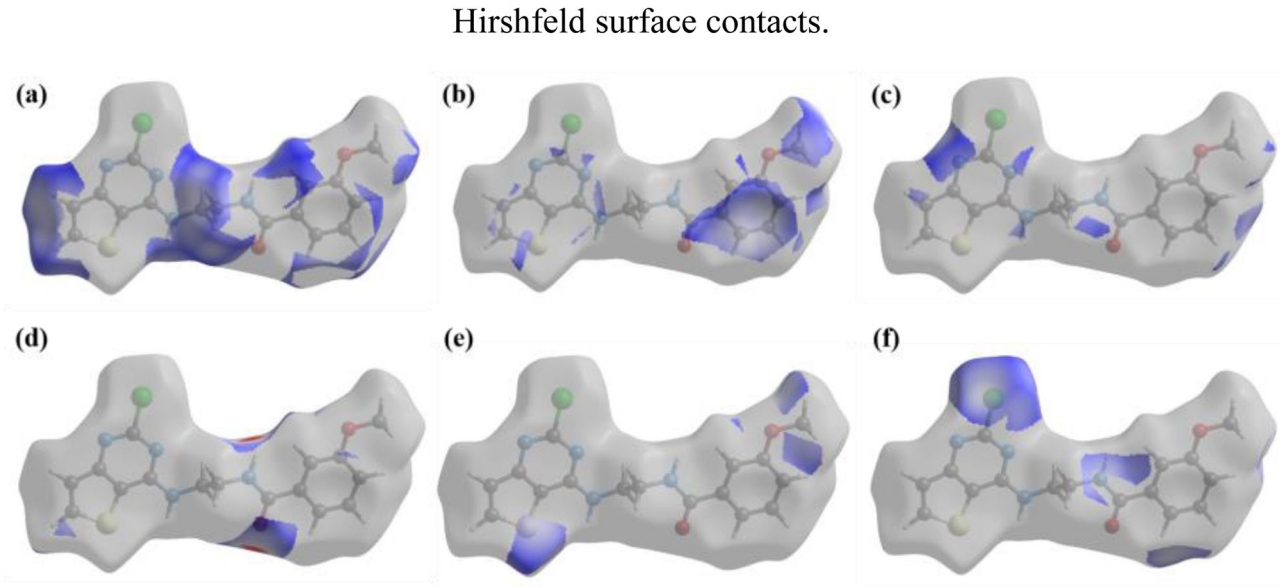

Figure 7. The Hirshfeld surface representations with the function dnorm plotted onto the surface for (a) H···H, (b) H···C/C···H, (c) H···N/N···H, (d) H···O/O···H, (e) H···S/S···H and (f) H···Cl/Cl···H interactions.

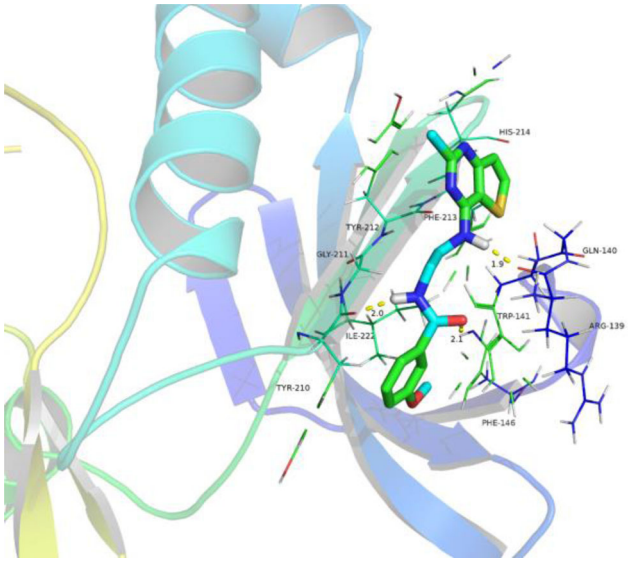

Figure 8. The molecular docking results of compound **8** with 3D15 protein.

confirmed by the single crystal X-ray diffraction studies. The X-ray crystallography characterization of the title compound was complemented by DFT calculations and Hirshfeld surface analysis. The density functional theory (DFT) optimized structure at the B3LYP/6-311 + G(d,p) method/basis set was compared with the experimentally determined molecular structure in the solid-state. Hirshfeld surface analysis and electrostatic potential (ESP) maps indicate that the major intermolecular contacts are between the hydrogen atoms of heteroatoms. In addition, the antitumor test of **8** shows significant activity against HT-29, A549 and MKN45 cell lines. Finally, the molecular docking studies revealed that the title compound may exhibit activity inhibiting PDB:3D15. This study may provide valuable information for the future design and development of antitumor agents with more potent activities. Studies on the mechanism of the action of the target compounds are in progress and will be reported in the future.

Disclosure statement

No potential conflict of interest was reported by the authors.

Funding

This work is supported by the team of syngas catalytic conversion of Shaanxi University of Technology, the national natural science foundation of China (project no. 21373132, 21603133, 21807068), project of education department of Shaanxi province (20JK0565, 20JK0552), Shaanxi provincial science and technology department project (2019JM471, 2020JM602), the project of Shaanxi University of Technology(SLGKY2009), the Young Talent fund of University Association for Science and Technology in Shaanxi, China (20180607).

References

Anderson, A. C. (2003). The process of structure-based drug design. *Chemistry & Biology*, *10*(9), 787–797. https://doi.org/10.1016/j.chembiol.2003.09.002

Barakat, A., Al-Majid, A. M., Soliman, S. M., Mabkhot, Y. N., Ali, M., Ghabbour, H. A., Fun, H. K., & Wadood, A. (2015). Structural and spectral investigations of the recently synthesized chalcone (E)-3-mesityl1-(naphthalen-2-yl) prop-2-en-1-one, a potential chemotherapeutic agent. *Chemistry Central Journal*, *9*, 1–15. https://doi.org/10.1186/s13065-015-0112-5

Bassetto, M., Leyssen, P., Neyts, J., Erukhimovich, M. M., Frick, D. N., & Brancale, A. (2016). Computer-aided identification, synthesis and evaluation of substituted thienopyrimidines as novel inhibitors of HCV replication. *European Journal of Medicinal Chemistry*, *123*, 31–47. https://doi.org/10.1016/j.ejmech.2016.07.035

Becke, A. D. (1993). Density-functional thermochemistry. III. The role of exact exchange. *Journal of Chemical Physics*, *98*(7), 5648–5652. https://doi.org/10.1063/1.464913

Bravo-Altamirano, K., George, K. M., Frantz, M. C., LaValle, C. R., Tandon, M., Leimgruber, S., Sharlow, E. R., Lazo, J. S., Wang, Q. J., & Wipf, P. (2011). Synthesis and structure-activity relationships of benzothienothiazepinone inhibitors of protein kinase D. *ACS Medicinal Chemistry Letters*, *2*(2), 154–159. https://doi.org/10.1021/ml100230n

Dabrowska, J., & Brylinski, M. (2006). Stereoselectivity of 8-OH-DPAT toward the serotonin 5-HT1A receptor: Biochemical and molecular modeling study. *Biochemical Pharmacology*, *72*(4), 498–511. https://doi.org/10.1016/j.bcp.2006.05.008

Dilly, S., & Liegeois, J. F. (2016). Structural insights into 5-HT1A/D4 selectivity of WAY-100635 analogues: Molecular modeling, synthesis, and in vitro binding. *Journal of Chemical Information and Modeling*, *56*(7), 1324–1331. https://doi.org/10.1021/acs.jcim.5b00753

Dörsam, B., & Fahrer, J. (2016). The disulfide compound α-lipoic acid and its derivatives: A novel class of anticancer agents targeting mitochondria. *Cancer Letters*, *371*(1), 12–19. https://doi.org/10.1016/j.canlet.2015.11.019

Duan, Y., Wu, C., Chowdhury, S., Lee, M. C., Xiong, G., Zhang, W., Yang, R., Cieplak, P., Luo, R., Lee, T., Caldwell, J., Wang, J., & Kollman, P. (2003). A point-charge force field for molecular mechanics simulations of proteins based on condensed-phase quantum mechanical calculations. *Journal of Computational Chemistry*, *24*(16), 1999–2012. https://doi.org/10.1002/jcc.10349

El-Sayed, W. A., Ali, O. M., Zyada, R., Mohamed, A. A., & Abdel-Rahman, A. (2012). Synthesis and antimicrobial activity of new substituted thienopyrimidines, their tetrazolyl and sugar derivatives. *Acta Poloniae Pharmaceutica*, *69*(3), 439–447.

Farce, A., Loge, C., Gallet, S., Lebegue, N., Carato, P., Chavatte, P., Berthelot, P., & Lesieur, D. (2004). Docking study of ligands into the colchicine binding site of tubulin. *Journal of Enzyme Inhibition and Medicinal Chemistry*, *19*(6), 541–547. https://doi.org/10.1080/14756360412331280545

Folkes, A. J., Ahmadi, K., Alderton, W. K., Alix, S., Baker, S. J., Box, G., Chuckowree, I. S., Clarke, P. A., Depledge, P., Eccles, S. A., Friedman, L. S., Hayes, A., Hancox, T. C., Kugendradas, A., Lensun, L., Moore, P., Olivero, A. G., Pang, J., Patel, S., … Shuttleworth, S. J. (2008). The identification of 2-(1H-indazol-4-yl)-6-(4-methanesulfonyl-piperazin-1-ylmethyl)-4-morpholin-4-yl-thieno[3,2-d]pyrimidine (GDC-0941) as a potent, selective, orally bioavailable inhibitor of class I PI3 kinase for the treatment of cancer. *Journal of Medicinal Chemistry*, *51*(18), 5522–5532. https://doi.org/10.1021/jm800295d

Frisch, M. J., Trucks, G. W., Schlegel, H. B., Scuseria, G. E., Robb, M. A., Cheeseman, J. R., Scalmani, G., Barone, V., Mennucci, B., Petersson, G. A., Nakatsuji, H., Caricato, M., Li, X., Hratchian, H. P., Izmaylov, A. F., Bloino, J., Zheng, G., Sonnenberg, J. L., Hada, M., … Fox, D. J. (2009). *Gaussian 09, Revision C.01*. Gaussian, Inc.

Gilbert, D. (2004). Bioinformatics software resources. *Briefings in Bioinformatics*, *5*(3), 300–304. https://doi.org/10.1093/bib/5.3.300

Hartwar, V. R., Sist, M., Jorgensen, M. R. V., Mamakhel, A. H., Wang, X., Hoffmann, C. M., Sugimoto, K., Overgaard, J., & Iversen, B. B. (2015). Quantitative analysis of intermolecular interactions in orthorhombic rubrene. *IUCrJ*, *2*, 563–574. http://dx.doi.org/10.1107/S2052252515012130

Heffron, T. P., Berry, M., Castanedo, G., Chang, C., Chuckowree, I., Dotson, J., Folkes, A., Gunzner, J., Lesnick, J. D., Lewis, C., Mathieu, S., Nonomiya, J., Olivero, A., Pang, J., Peterson, D., Salphati, L., Sampath, D., Sideris, S., Sutherlin, D. P., … Zhu, B. (2010). Identification of GNE-477, a potent and efficacious dual PI3K/mTOR inhibitor. *Bioorganic & Medicinal Chemistry Letters*, *20*(8), 2408–2411. https://doi.org/10.1016/j.bmcl.2010.03.046

Humphrey, W., Dalke, A., Schulten, K., & Molec, V. J. (1996). VMD: Visual molecular dynamics. *Journal of Molecular Graphics*, *14*(1), 33–38. https://doi.org/10.1016/0263-7855(96)00018-5

Ji, X. H., Zhao, J., Lu, J. F., Jin, L. X., & Ge, H. G. (2019). Synthesis, Crystal Structure and Biological Activity of 1-(3-Amino-4-morpholino-1H-indazole-1-carbonyl)-N-(4-fluorophenyl)cyclopropane-1-carboxamide. *Chinese Journal of Structural Chemistry*, *38*, 1889–1894. https://doi.org/10.14102/j.cnki.0254-5861.2011-2372

Kang, D. W., Fang, Z. G., Li, Z. Y., Huang, B. S., Zhang, H., Lu, X. Y., Xu, H. R., Zhou, Z. X., Ding, X., Daelemans, D., Clercq, E. D., Pannecouque, C., Zhan, P., & Liu, X. Y. (2016). Design, synthesis, and evaluation of thiophene[3,2-d]pyrimidine derivatives as HIV-1 non-nucleoside reverse transcriptase inhibitors with significantly improved drug resistance profiles. *Journal of Medicinal Chemistry*, *59*(17), 7991–8007. https://doi.org/10.1021/acs.jmedchem.6b00738

Kotaiah, Y., Harikrishna, N., Nagaraju, K., & Rao, C. V. (2012). Synthesis and antioxidant activity of 1,3,4-oxadiazole tagged thieno[2,3-d]pyrimidine derivatives. *European Journal of Medicinal Chemistry*, *58*, 340–345. https://doi.org/10.1016/j.ejmech.2012.10.007

Lee, C., Yang, W., & Parr, R. G. (1988). Development of the Colle-Salvetti correlation-energy formula into a functional of the electron density. *Physical Review. B, Condensed Matter*, *37*(2), 785–789. https://doi.org/10.1103/physrevb.37.785

Liu, J., Shi, J. T., Hao, X. C., Liu, Y. T., Ding, S., Wang, Y., & Chen, Y. (2019). Synthesis of New Substitut2-amino-4H-benzo[h]chromene-3-carbonitrile Derivatives. *Journal of the Chemical Society of Pakistan*, *41*, 888–892.

Lu, J. F., Jin, L. X., Ge, H. G., Ji, X. H., Guo, X. H., Tian, G. H., Song, J., & Jiang, M. (2017). Synthesis, Crystal, Computational Study and Biological Activity of N-(1-(2,4-Dichlorophenyl)-1H-pyrazolo[3,4-d]pyrimidin-4-yl)-4-(N,N-dipropylsulfamoyl)benzamide. *Chinese Journal of Structural Chemistry*, *36*, 1810–1816. https://doi.org/10.14102/j.cnki.0254-5861.2011-1668.

Lu, J. F., Zhou, X. L., Xu, Y. H., Yue, S. Y., Ji, X. H., Zheng, N., & Jin, L. X. (2017). Synthesis, crystal structure, and biological activity of 3-amino-4-morpholino-N-[2-(trifluoromethoxy)phenyl]-1H-indazole-1-carboxamide. *Journal of Chemical Research*, *41*(9), 526–528. https://doi.org/10.3184/174751917X15033157981988

Lu, T., & Chen, F. (2012). Multiwfn: A multifunctional wavefunction analyzer. *Journal of Computational Chemistry*, *33*(5), 580–592. https://doi.org/10.1002/jcc.22885

Mckinnon, J. J., Spackman, M. A., & Mitchell, A. S. (2004). Novel tools for visualizing and exploring intermolecular interactions in molecular crystals. *Acta Crystallographica. Section B, Structural Science*, *60*(Pt 6), 627–668. https://doi.org/10.1107/S0108768104020300

Morris, G. M., Huey, R., Lindstrom, W., Sanner, M. F., Belew, R. K., Goodsell, D. S., & Olson, A. J. (2009). AutoDock4 and AutoDockTools4: Automated docking with selective receptor flexibility. *Journal of Computational Chemistry*, *30*(16), 2785–2791. https://doi.org/10.1002/jcc.21256

Rizk, O. H., Shaaban, O. G., & El-Ashmawy, I. M. (2012). Design, synthesis and biological evaluation of some novel thienopyrimidines and fused thienopyrimidines as anti-inflammatory agents. *European Journal of Medicinal Chemistry*, *55*, 85–93. https://doi.org/10.1016/j.ejmech.2012.07.007

Sakthivel, S., Alagesan, T., Muthu, S., Abraham, C. S., & Geetha, E. (2018). Quantum mechanical, spectroscopic study (FT-IR and FT - Raman), NBO analysis, HOMO-LUMO, first order hyperpolarizability and docking studies of a non-steroidal anti-inflammatory compound. *Journal of Molecular Structure*, *1156*, 645–656. https://doi.org/10.1016/j.molstruc.2017.12.024

Sheldrick, G. M. (1997). *SHELXS-97, Program for the solution of crystal structures*. University of Göttingen.

Shi, J. T., Gong, Y. L., Li, J., Wang, Y., Chen, Y., Ding, S., & Liu, J. (2019). Synthesis, Structure and Biological Activity of 2-[2-(4-Fluorobenzylidene)hydrazinyl]-4-(1-methyl-1H-indol-3-yl)thieno[3,2-d]pyrimidine*Chinese Journal of Structural Chemistry*, *38*, 1530–1536. https://doi.org/10.14102/j.cnki.0254-5861.2011-2410

Sıdır, İ., Sıdır, Y. G., Kumalar, M., & Taşal, E. (2010). Ab initio Hartree–Fock and density functional theory investigations on the conformational stability, molecular structure and vibrational spectra of 7-acetoxy-6-(2,3-dibromopropyl)-4,8-dimethylcoumarin molecule. *Journal of Molecular Structure*, *964*(1-3), 134–151. https://doi.org/10.1016/j.molstruc.2009.11.023

Sutherlin, D. P., Sampath, D., Berry, M., Castanedo, G., Chang, Z., Chuckowree, I., Dotson, J., Folkes, A., Friedman, L., Goldsmith, R., Heffron, T., Lee, L., Lesnick, J., Lewis, C., Mathieu, S., Nonomiya, J., Olivero, A., Pang, J., Prior, W. W., … Zhu, J. (2010). Discovery of (thienopyrimidin-2-yl)aminopyrimidines as potent, selective, and orally available pan-PI3-kinase and dual pan-PI3-kinase/mTOR inhibitors for the treatment of cancer. *Journal of Medicinal Chemistry*, *53*(3), 1086–1097. https://doi.org/10.1021/jm901284w

Turner, M. J., McKinnon, J. J., Wolff, S. K., Grimwood, D. J., Spackman, P. R., Jayatilaka, D., & Spackman, M. A. (2017). *CrystalExplorer17*. The University of Western Australia.

Zhou, L., Hu, Q., Chai, L. Q., Mao, K. H., & Zhang, H. S. (2019). X-ray characterization, spectroscopic, DFT calculations and Hirshfeld surface analysis of two 3-D supramolecular mononuclear zinc(II) and trinuclear copper(II) complexes. *Polyhedron*, *158*, 102–116. https://doi.org/10.1016/j.poly.2018.10.052